

REPORT DOCUMENTATION PAGE			Form Approved OMB NO. 0704-0188		
<p>The public reporting burden for this collection of information is estimated to average 1 hour per response, including the time for reviewing instructions, searching existing data sources, gathering and maintaining the data needed, and completing and reviewing the collection of information. Send comments regarding this burden estimate or any other aspect of this collection of information, including suggestions for reducing this burden, to Washington Headquarters Services, Directorate for Information Operations and Reports, 1215 Jefferson Davis Highway, Suite 1204, Arlington VA, 22202-4302. Respondents should be aware that notwithstanding any other provision of law, no person shall be subject to any penalty for failing to comply with a collection of information if it does not display a currently valid OMB control number. PLEASE DO NOT RETURN YOUR FORM TO THE ABOVE ADDRESS.</p>					
1. REPORT DATE (DD-MM-YYYY) 31-08-2009		2. REPORT TYPE Final Report		3. DATES COVERED (From - To) 7-May-2007 - 31-Jul-2008	
4. TITLE AND SUBTITLE Novel mode of nucleation and growth of complex oxide heterostructures at the extreme of high supersaturation. Effects of orbital reconstruction.			5a. CONTRACT NUMBER W911NF-07-1-0273		
			5b. GRANT NUMBER		
			5c. PROGRAM ELEMENT NUMBER 611102		
			5d. PROJECT NUMBER		
6. AUTHORS Jak Tchakhalian			5e. TASK NUMBER		
			5f. WORK UNIT NUMBER		
7. PERFORMING ORGANIZATION NAMES AND ADDRESSES University of Arkansas Board of Trustees University of Arkansas Fayetteville, AR 72701 -			8. PERFORMING ORGANIZATION REPORT NUMBER		
9. SPONSORING/MONITORING AGENCY NAME(S) AND ADDRESS(ES) U.S. Army Research Office P.O. Box 12211 Research Triangle Park, NC 27709-2211			10. SPONSOR/MONITOR'S ACRONYM(S) ARO		
			11. SPONSOR/MONITOR'S REPORT NUMBER(S) 52877-PH.1		
12. DISTRIBUTION AVAILABILITY STATEMENT Approved for public release; Distribution Unlimited					
13. SUPPLEMENTARY NOTES The views, opinions and/or findings contained in this report are those of the author(s) and should not be construed as an official Department of the Army position, policy or decision, unless so designated by other documentation.					
14. ABSTRACT We report on a detailed investigation of the kinetics of thin-film condensation and switching scaling behavior upon large lattice mismatch and extremely high supersaturation, which is exemplified by novel class of complex oxide heterostructures composed of a correlated metal RENiO ₃ (RE=La,Nd,Pr) and wide-gap dielectric LaAlO ₃ (LAO) grown on SrTiO ₃ (001) single crystals. In sharp contrast to conventional PLD and MBE growth, the single unit cell growth data acquired by specular and diffuse RHEED reflectivity have revealed the presence of an unusual					
15. SUBJECT TERMS artificial complex oxide heterostructures, exotic magnetism and superconductivity					
16. SECURITY CLASSIFICATION OF:			17. LIMITATION OF ABSTRACT SAR	15. NUMBER OF PAGES	19a. NAME OF RESPONSIBLE PERSON Jak Tchakhalian
a. REPORT U	b. ABSTRACT U	c. THIS PAGE U			19b. TELEPHONE NUMBER 479-575-4313

DOD Funding Report - W911NF0810186

by Jak Tchakhalian

with Michel Kareev (PDF), Jian Liu (PhD) and Benjamin Gray (PhD)

August 31, 2009

1. Novel mode of nucleation and growth of complex oxide heterostructures at the extreme of high supersaturation.

Statement of problem. Since the theoretically predicted exotic superconductivity and magnetism puts extremely stringent requirements for the thickness of a layer being in proximity to the interface, we immediately confronted a problem of fabrication of the unit-cell thick LNO/LAO heterostructures with the LaNiO_3 (LNO) layer metallicity maintained down to 1-3 unit cells. Recap that in accordance with the Ioffe-Altschuller-Anderson theory, the susceptibility of a metallic system to disorder falls very rapidly with its dimensionality. From the fabrication point of view this means that we must maintain an exquisite level of control over oxygen and cation defects or disorder in general to prepare heterostructures suitable for experiments. To circumvent the issue we developed a completely new growth mode, which enables us to produce high-quality ultra-thin epitaxial heterostructures. In what follows are the details of the new growth method.

Solution. During the past several years, extensive work on pulsed laser deposition (PLD) combined with high pressure RHEED opened up new and exciting prospects for the stabilization of unusual metastable phases of materials that are generally not achievable by other techniques relying on slow growth kinetics[1-7, 8]. In the past, PLD growth parameters are subjected to rigorous phenomenological investigation with the aim to obtain a layer-by-layer (LBL) growth. Evidently, the complexity of growth increases many-fold for heterostructures composed of diverse layers with often-antagonistic electronic, magnetic and structural properties and subjected to a large magnitude of strain and confined dimensions. Among the fundamentally important issues, the early stage of nucleation and condensation of a new multi-component phase at the extreme of large supersaturation (SS) are the least investigated to date[9, 10, 11]. In particular, its evolution with time and temperature and the possible switching of growth mechanisms during the single unit cell formation [12, 13] are not well understood.

In this document, we report on a detailed investigation of the kinetics of thin-film condensation and switching scaling behavior upon large lattice mismatch and extremely high supersaturation (SS), which is exemplified by the novel class of complex oxide heterostructures composed of a correlated metal RENiO_3 (RENO, RE=La,Nd,Pr) and wide-gap dielectric LaAlO_3 (LAO). The $[n \text{ RENO}/m \text{ LAO}]_x N$ superlattices (SL), where n and m are the numbers of unit cells and N denotes the number of periods, were grown by PLD on atomically flat TiO_2 terminated (001) SrTiO_3 (STO) single crystals, which were prepared by our recently developed wet-etch

procedure[15] to minimize electronic surface and near-surface defects. In the following, we focus on a representative RE=La subclass of these SLs.

For the project our PLD system was substantially redesigned and equipped with a newly developed high pressure RHEED, which is capable of operating in the background oxygen pressure of up to 400 mTorr, with an advanced feedback control of the current and a custom developed 12-bit high-speed imaging system with a timing resolution of $\lesssim 20$ msec. We employ a real-time 3D imaging mode to monitor both specular and diffuse intensities within a large portion of the momentum space and per laser pulse. By recording the temporal evolution of the diffracted intensity during the growth, we can obtain details on the development of surface morphology and atomic structure including changes in surface disorder, defects formation, agglomeration of islands, and step bunching [14].

In growing epitaxial heterostructures, it is common to monitor the time dependence of the RHEED specular intensity (RSI) in order to characterize the quality of the coverage during *continuous* deposition. In the ideal case, the RSI exhibits characteristic oscillations attesting to a LBL deposition. Figure 1(A-C) shows the result of a typical *continuous* deposition of a 4 u.c. thick layer of LNO on STO with an imposed slow growth rate, which is set by the laser frequency of 3 Hz. As clearly seen, the RSI exhibits strong damping right after a few monolayers, which is inherent of rapidly increasing surface disorder. The diffuse intensity shown in Fig. 1(C) exhibits a series of pronounced peaks with a transmission pattern through microcrystalline 3D-like islands[16, 17, 18], which is characteristic of the Volmer-Weber or the Stransky-Krastanov mode. The AFM large area scans further corroborate the presence of pronounced 3D structures on the surface. However, upon increasing the deposition rate up to 30 pulses/sec and introducing a prolonged delay time up to 120 seconds between two consecutive unit cells, the resulting nucleation and growth undergoes dramatic changes. As shown in Figs 1(D-F) and A1, excellent LBL growth is obtained and yields high-quality SLs with excellent morphological and electronic properties.

To elucidate the origin of such an unusual and profound change in the kinetics of nucleation and growth, we performed detailed temporal and temperature dependent studies (480°C to 780°C) on the surface coverage during the growth of a single unit cell. Upon examination of the RSI, oscillations in Fig. 2(A) are found to be asymmetric around the minimum point, which is in marked contrast to the conventional ‘parabolic’ shape found in a slow deposition rate growth. The asymmetry strongly testifies to the limited kinetics behavior due to changes in configuration or disorder beyond a singular scaling law during the unit-cell growth[19, 20]. Figure 2(A) shows the oscillations during the unit-cell growth at different temperatures under otherwise identical growth conditions. Surprisingly and contrary to the conventional models of 2D growth, the process of nucleation and condensation at high laser frequency shows a rather complex dependence on temperature. Specifically, the initial stage of deposition (area 1 in Fig. 2(A)) is *T-independent* and is followed by a non-linear T-dependence in the recovery area 2. Finally, at the saturation (area 3), the RSI switches its T-dependence again. A similar transformation in the growth law can be seen in the changes of scaling of the RSI with temperature presented in Fig. A2.

The absence of T-dependence in the initial stage is completely unexpected, since the theories of 2D growth including those with the step flow[21] rely on T-controlled diffusion for the nucleation and growth of adatom clusters. Moreover, one would expect a strong *T*-dependence from 450°C to 780°C, because temperature enters the nucleation barrier exponentially which local fluctuations overcome upon ablation to condensate a new phase in the metastable state

according to the classical thermodynamical framework. Thus, the origin of this unusual behavior must associate with the specifics of nucleation at an extremely large degree of SS, which is produced by a combination of short laser pulses of 20 ns and a high pulse-rate up to 20-30 Hz[22, 23]. The correspondingly high nucleation rate results in a critical nucleus radius $i_c \approx 1-2$ (the extreme limit) and the invalidity of conventional models of nucleation[24, 25, 26] including the atomistic Walton model[27]. Specifically, since $i_c \approx 1-2$, the new-phase clusters cannot be unambiguously defined. The surface and the internal volume become comparable in size with the fluctuations, which now affect the whole nucleus and not only its boundaries. Consequently, the internal structure of a critical nucleus is rendered unstable and is subjected to changes during the fluctuations. As a result, the fundamental parameters describing the metastable system such as interfacial energy, diffusion coefficient, and hopping frequency are *a priori* ill defined. Instead, at this limit of the thermodynamic instability (i.e near the spinodal) a new-phase transformation proceeds through the activation free (i.e. T-independent) relaxation of the strongly metastable vapor phase by means of the spinodal decomposition (SD)[28, 29, 30]. Therefore, the observed scaling behavior during the stage 1 and the characteristic spatial distribution of islands in Fig 2(C) strongly suggest that the initially metastable vapor spontaneously transforms into a new-phase of strongly interacting clusters and proceeds with the rapid decrease of free energy without the nucleation barrier. Since the new-phase formation is barrier free, the SD process is likely to proceed significantly faster than the conventional nucleation. Thus its transitional kinetics is beyond the millisecond timescale of the RHEED[31, 32]. Another important observation, which additionally contributes to the *T*-independence of the stage 1, is that the supersaturated vapor is thermodynamically decoupled from the substrates, which are heated to much lower temperatures than the ablated material, which is on the order of eV[33, 34].

From the experimental point of view, the kinetics of nucleation can be conveniently controlled by the laser pulse frequency as follows. First, a significant increase in the laser frequency pumps the ablated material into the vicinity of the substrate and thus enlarges the SS that scales with the mass density. Secondly, the magnitude of SS critically defines the mechanism of relaxation of the supersaturated adatom population and either facilitates the ease of nucleation (low SS) or for a sufficiently high pulse-rate acts to bound the critical radius to a single particle via the spinodal decay.

At the second stage of the unit-cell condensation, which is marked in Fig. 2(A) as t_M , when the Gibbs energy is reduced via the formation of the new phase islands, the substrate temperature (T_s) becomes the prime driving force in the kinetics of growth and eventual thin-film layer formation. Thus, the RSI oscillations will result from the T-controlled competition between cluster formation and step propagation. To check the validity of the described scenario, we calculated the surface coverage, θ and roughness, Δ in the framework of the bilayer model [[11, 35, 36]] to reveal their dependency on critical growth parameters such as T_s and dwell time. The general expression connecting the RSI $I(t)$ and the coverage $\theta(t)$ is written as [[11]] $I(t)=I_0[1-2\theta_1(t)+2\theta_2(t)]^2$, here θ_1 and θ_2 are the time-dependent coverages of the first and the second atomic layers, respectively, and I_0 is a scaling factor depending on the laser power density and specific thermodynamic conditions. In addition, the coverage is constrained to $\theta_1(t)+\theta_2(t)=mt$, where m is the deposition rate, which vanishes as laser is off (i.e. $m=0$ at $t>t_E$). Next, we set $mt_E=1$ implying that θ_2 , if finite during the deposition phase, is supposed to vanish during the

dwel time. The corresponding roughness can be calculated according to the following expression $\Delta(t) = \sqrt{\theta_1(t)(1-\theta_1(t)-\theta_2(t))^2 + \theta_2(t)(2-\theta_1(t)-\theta_2(t))^2}$. Under these conditions, the experimental RSI can be used to obtain θ_1 , θ_2 and Δ as a function of time and the T s.

The results of the theoretical treatment are presented in Figs. 3 (A-C). As anticipated for all the temperatures, the coverage of the first layer increases linearly with the deposition time. Also, in accordance with the experimental observation during the initial phase 1 the initial slope of the $\theta_1(t, T)$ curves is T -independent (see Figs. 3(A) and A2). On the other hand, the second layer coverage θ_2 starts showing some T -dependence as the RSI approaches its lowest value at t_M . In addition, the roughness, Δ shown in Fig. 3(B) increases rapidly and steadily from the very beginning, which is another signature for the SD process[28, 29, 30]. Therefore, we conclude that at phase 1, the high degree of SS is dominant over the T s and is crucial for the high quality growth.

Starting from the point t_M , the data obtained between 450°C and 780°C differs largely. The heterostructures grown at temperatures around 700°C and above continue the main trend in the phase 1, namely the coverage θ_1 continues increasing. At the same time the second layer coverage θ_2 declines rapidly. In sharp contrast, for the samples grown at 450°C to 580°C, θ_1 becomes progressively slower, and instead θ_2 continues its strong progression. These behaviors indicate that diffusion over the surface clearly becomes a key factor to maintain 2D growth as opposed to developing 3D islands inherent to the colder deposition. The strong T -dependence of θ_2 also suggests that for the high T s the occasionally grown second level can rapidly relax to the first level. Whereas for colder deposition this T -controlled process is suppressed leading to the rapidly increasing roughness. Consequently, strong evidence for the new scaling law can be deduced from an analysis of the T -dependence of the RSI after t_M . As clearly seen in Fig. A2, the T -independent scaling law found in phase 1 is now switched to an exponential dependence on $1/T$ in accord with the Walton atomistic model[27]. This marked difference can be also explicated from the observation that at t_M , θ_1 reaches a value close to 0.5. This specific value is known as being critical in the 2D percolation problem[22, 37]. This new spatial arrangement is thus characterized by the developing long-range order parameter as evidenced by the recovering RSI and from the characteristic spatial pattern of islands shown in Fig 2(C).

Upon completion of the ablation process at t_E labeled as phase 3 in Fig. 3(A), the temporal dependence of the coverage changes again. During the relaxation period, θ_2 starts decreasing while the first layer recovers at the expense of the second layer. However, this recovery is strongly T -dependent, namely, for low temperature deposition the first layer does not recover in full, whereas at 700°C and above it restores to its maximum magnitude. Conversely, the low- T deposition results in 3D islands formation as confirmed by AFM shown in Fig. A3. During this phase, the disorder configuration reflected in the scaling behavior of the diffracted intensity undergoes yet another marked change from the exponential behavior to the power law, as illustrated in Fig. S2.

Indeed, the time evolution of the layer coverage can be derived analytically. One can detail the kinetics of the second layer coverage as follows, $\frac{d\theta_2(t)}{dt} = \lambda\theta_1(t) - \frac{1}{\tau}\theta_2(t)$ (Eqn. 3). Here the first term implies that the coverage of the second layer scales with the surface of the first layer since the second layer cannot develop in the vacuum. The second term describes the relaxation of the second layer. Correspondingly, this model involves two phenomenological parameters, λ and τ . The kinetics of the first layer coverage is trivially obtained from Eqn.(3). This model has an analytical solution, which for $t < t_E$ reads $\theta_2^{(1)}(t) = \frac{\lambda m}{\alpha} t - \frac{\lambda m}{\alpha^2} [1 - e^{-\alpha t}]$, where $\alpha = \lambda + 1/\tau$. Next, we expand this expression in a series with respect to t , which results in the first non-zero term $\theta_2(t < t_E) \propto t^2$. During the dwell time ($m=0$) Eqn. (3) yields the exponentially decreasing coverage $\theta_2^{(2)}(t) = \theta_2^{(1)}(t_E) e^{-\alpha(t-t_E)}$. As before, the corresponding first layer coverage can be easily obtained from Eqn. (3). Thus, the model predicts that initially $\theta_1(t)$ increases linearly while $\theta_2(t)$ increases quadratically with time. After $t = t_E$, $\theta_1(t)$ continue growing whereas $\theta_2(t)$ rapidly decreases. These model predictions are in excellent agreement with the obtained experimental results.

Summary. We have fabricated and investigated the PLD growth of a novel class of complex oxide SLs composed of a correlated metal RENO - wide band-gap dielectric LAO under the large tensile strain and at the limit of high SS. *We have demonstrated the importance of a new and unexplored mode of the LBL growth at the extreme of metastability to produce high-quality complex oxide multilayers, which paves a way to the LBL growth of novel ultra-thin complex oxide heterostructures otherwise not attainable by conventional growth methods.* More specifically, we have found that upon approaching the metastability point, the unit-cell growth evolves through three profoundly different growth laws characterized by the distinct temporal and temperature scaling behaviors. We have shown, that the first and most critical growth phase is T-independent, implying that it proceeds through a mechanism analogous to spinodal decay of a strongly metastable system. This behavior is controlled by thermodynamics and not by kinetics. After the coverage reaches 0.5, the growth law then changes to a T-controlled phase characterized by the appearance of a new order parameter and attributed to the formation of an infinite 2D cluster of the new material phase. The final recovery phase, is controlled by the mass- and distance- limited diffusion, which smoothes the layer structure by means of the relaxation of the particles from the top of the new layer to the holes within the bottom layer.

References for part 1.

- [1] A. Ohtomo *et al.*, Nature **419**, 378 (2002).
- [2] Y.-H Chu *et al.*, Nat. Mater. **7**, 478 (2008).
- [3] J. Chakhalian *et al.*, Science **318**, 1114 (2007).
- [4] A. Ohtomo and H. Y. Hwang, Nature **427**, 423 (2004).
- [5] S.-W. Cheong and M. Mostovoy, Nat. Mater. **6**, 13 (2007); T. Kimura *et al.*, *ibid.* **7**, 291 (2008).
- [6] J. Chaloupka and G. Khaliullin, Phys. Rev. Lett. **100**, 016404 (2008).
- [7] M. A. Herman, W. Richter and H. Sitter, *Epitaxy: Physical Foundation and Technical Implementation*(Springer, New York, 2004).
- [8] K. S. Sree Harsha, *Principles of Vapor Deposition of Thin Films*(Elsevier, New York, 2006).
- [9] G. Koster *et al.*, Appl. Phys. Lett. **74**, 3729 (1999).

- [10] D. H. A. Blank *et al.*, *J. Cryst. Growth* **211**, 98 (2000).
- [11] J. Z. Tschler *et al.*, *Phys. Rev. Lett.* **96**, 226104 (2006).
- [12] S. A. Kukushkin and A. V. Osipov, *Physics-Uspekhi* **41**, 983 (1998); F. M. Kuni, A. K. Shchekin and A. P. Grinin, *ibid.* **44**, 331 (2001).
- [13] S. A. Kukushkin and A. V. Osipov, *J. Phys. Chem. Solids* **56**, 831 (1995).
- [14] W. Hong *et al.*, *Phys. Rev. Lett.* **95**, 095501 (2005).
- [15] M. Kareev *et al.*, *Appl. Phys. Lett.* **93**, 061909 (2008); J. Zhang *et al.*, *ibid.* **94**, 092904 (2009).
- [16] A.Y. Cho, *J. Cryst. Growth* **201/202**, 1 (1999).
- [17] X. H. Wei *et al.*, *J. Phys. D: Appl. Phys.* **40**, 7502 (2007).
- [18] G. Koster, Ph. D. thesis, Univ. of Twente.
- [19] G. Lagally, D. E. Savage, and M. C. Tringides, in *Reflection High-Energy Electron Diffraction and Reflection Electron Imaging of Surfaces*, edited by P. K. Larsen and P. J. Dobson (Plenum, New York, 1988), p. 138.
- [20] M. C. Tringides and M. G. Lagally, *Surf. Sci.* **195**, L159 (1988).
- [21] M. Lippmaa *et al.*, *Appl. Phys. Lett.* **74**, 3543 (1999); M. Lippmaa *et al.*, *ibid.* **76**, 2439 (2000).
- [22] G. Rosenfeld, B. Poelsema, and G. Comsa, in *Growth and Properties of Ultrathin Epitaxial Layers*, edited by D. A. King and D. P. Woodruff (Elsevier, New York, 1997), p. 66.
- [23] B. Chrisey and G. K. Hubler, *Pulsed Laser Deposition of Thin Films* (Wiley, New York, 1994).
- [24] E. Vasco and J. L. Sacedon, *Phys. Rev. Lett.* **98**, 036104 (2007); E. Vasco, C. Polop and J. L. Sacedon, *ibid.* **100**, 016102 (2008); P.R. Willmott *et al.*, *ibid.* **96**, 176102, (2006).
- [25] B. Shin and M. Aziz, *Phys. Rev. B* **76**, 085431, (2007).
- [26] X. Wang *et al.*, *Chin. Phys. Lett.* **25**, 663 (2008).
- [27] D. Walton, *J. Chem. Phys.* **37**, 2182 (1962).
- [28] R. Bruinsma and A. Zangwill, *Europhys. Lett.* **4**, 729 (1987).
- [29] S. Joly *et al.*, *Phys. Rev. Lett.* **77**, 4394 (1996).
- [30] A. V. Osipov, *J. Phys. D: Appl. Phys* **28**, 1670 (1995).
- [31] G. Eres *et al.*, *Appl. Phys. Lett.* **80**, 3379 (2002).
- [32] A. Fleet *et al.*, *Phys. Rev. Lett.* **96**, 055508 (2006).
- [33] D. Smith, *Thin-Film Deposition: Principles and Practice* (McGraw-Hill, New York, 1995).
- [34] A. Sambri, Ph. D. thesis, Univ. degli Studi di Napoli Federico II, 2008.
- [35] A. Ichimiya and P. I. Cohen, *Reflection High Energy Electron Diffraction* (Cambridge University Press, Cambridge, England, 2004).
- [36] P. I. Cohen *et al.*, *Surf. Sci.* **216**, 222 (1989).
- [37] S. Torquato, *Random Heterogeneous Materials: Microstructure and Macroscopic Properties* (Springer-Verlag, New York, 2005).

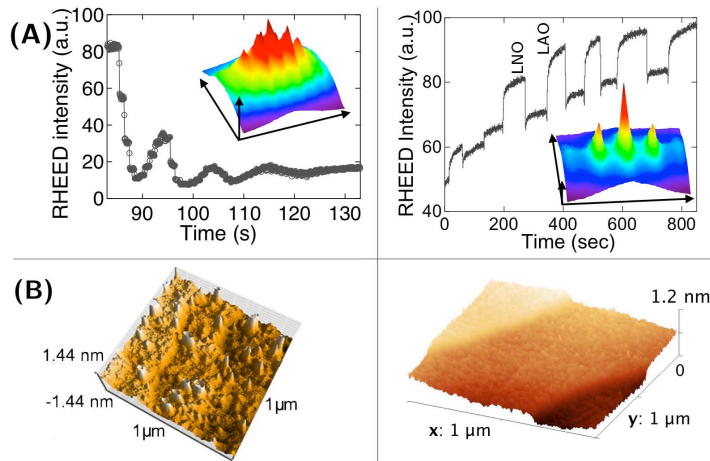


Figure 1: (Color online) (A) RHEED intensity oscillation during the growth of LNO/LAO SL ($n=4$) on STO (001) for slow rate of 3Hz and continuous deposition with a RHEED pattern characteristic 3D island formation. (B) the corresponding AFM image confirming the large degree of surface disorder. (C) RHEED diffuse scattering pattern characteristic of transmitted electrons through 3D like islands. Growth conditions are $T=730^{\circ}\text{C}$, $P_{\text{O}_2} \sim 100$ mTorr and the laser power density ~ 2.2 J/cm². (D)-(F) Upon increasing the laser frequency to 30Hz and introducing a prolong dwell-time of up to 120 secs, the deposition changes dramatically resulting in excellent LBL growth as seen from the corresponding RHEED and AFM images. Note, during the experiment, except for the pulse-rate, all other control parameters were kept identical.

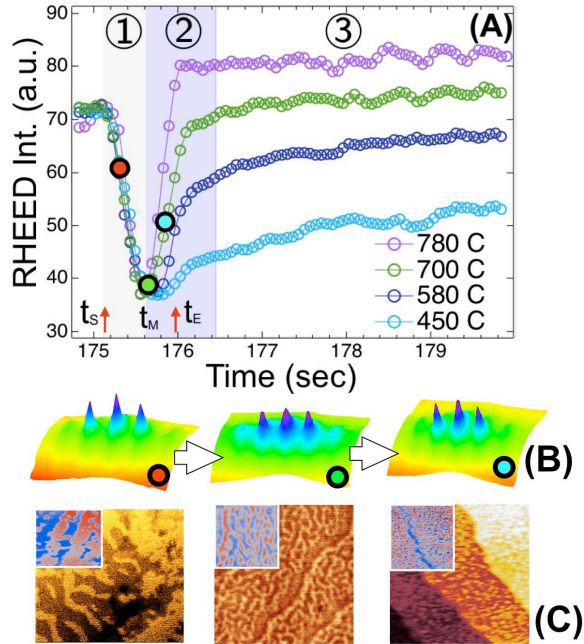
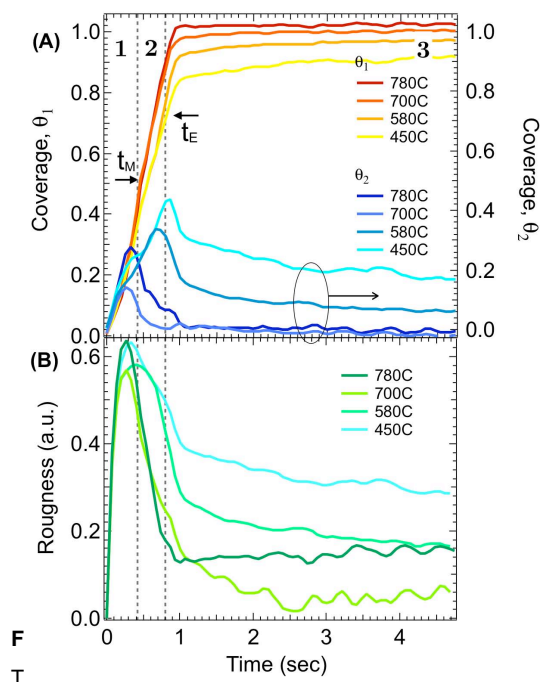


Figure 2: (Color online) (A) Dependence of the RHEED intensity on the growth temperature during the single unit cell growth per laser pulse. Three distinct phases 1-3 correspond to the markedly different growth laws. The red arrows indicate the start, t_s and the end, t_E of the ablation process (laser on and off). The lowest diffracted intensity is marked as t_M . (B) Evolution of the surface disorder with time as recorded by the diffuse RHEED. Red, green and blue circles correspond to 0.3, 0.5 and 0.7 coverage. (C) The real-space AFM images of surface at the same coverage obtained by interrupting the growth at the corresponding coverage. Since the evolution of disorder configuration during the phase 1 is independent of temperature, the laminae-like island pattern is roughly representative of the same surface seen by RHEED. The AFM scans with the field view of $1\mu\text{m}^2$ - $4\mu\text{m}^2$ are obtained in a dynamic mode with the phase contrast. Insets show the false-colored phase contrast images.



age, $\theta_{1,2}$ with the temperature and (B) corresponding layer roughness, Δ . Same time-intervals in Fig. 2(A).

Supplementary figures for part 1.

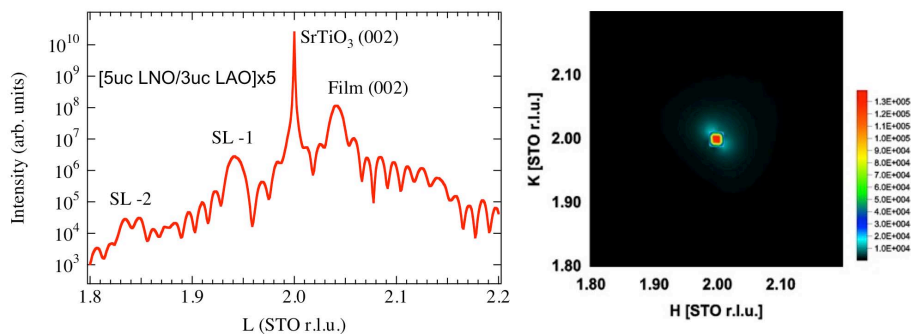


Figure 4: **Auxiliary Supplement:** (Color online) x-ray diffraction scan showing well defined superlattices peaks. The absence of any observed diffuse scattering additionally testifies for the high-quality epitaxial growth.

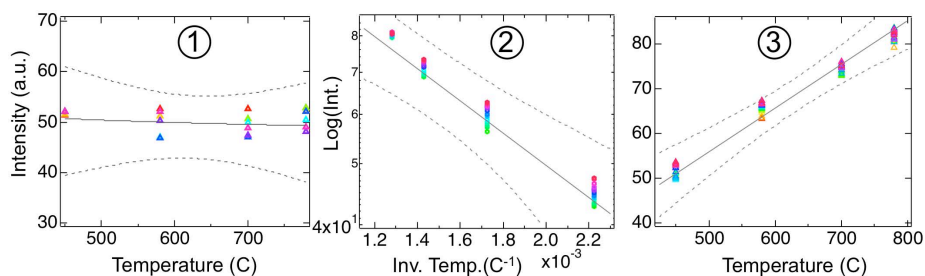


Figure 5: **Auxiliary Supplement:**(Color online) Scaling behavior of the RHEED intensity as a function of temperature showing three distinct phases (i.e. growth laws) during the unit cell formation. Solid line represents a fit to (1) linear T -dependence, (2) $\log(I) \propto (1/T)$

and (3) to the power law $I \propto T^\beta$. The corresponding to those numbers time-intervals are defined in Fig. 2(A). Dashed lines represent lower and upper confidence limits.

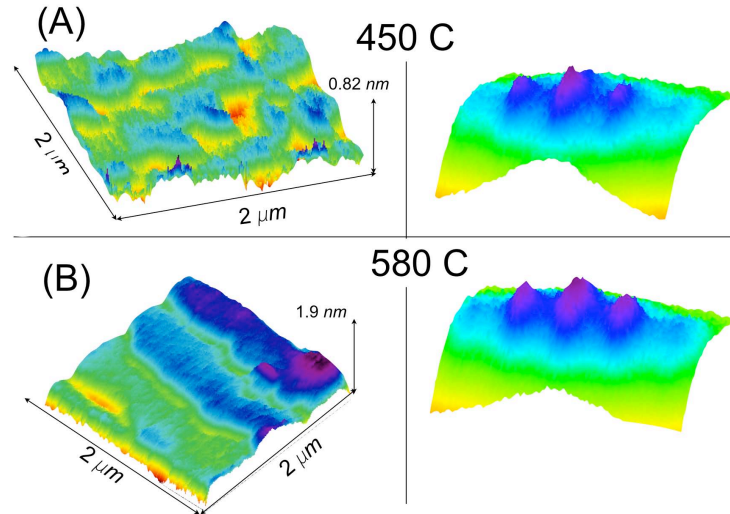


Figure 6: **Auxiliary Supplement:**(Color online) RHEED and AFM images of the surface for the low temperature deposition. The 3D island formation is clearly observed in this case.

2. Orbital reconstruction at the $\text{LaNiO}_3/\text{LaAlO}_3$ heterojunctions.

With the availability of high quality samples we proceeded toward characterization of their electronic and magnetic properties by polarized X-ray synchrotron radiation in soft energy regime (400 eV – 1400eV). First, we used XAS spectroscopy to track valencies of Ni by comparing the lineshape and position of the $L_{3,2}$ absorption with respect to the high-quality bulk powder reference sample provided by B. Dombrowski, Univ. of Chicago. Having developed strong confidence in the quality of the heterostructures including their structural and electronic properties, we used linearly polarized light to probe orbital reconstruction of the Ni eg electrons as predicted by the Khaliulin-Anderson model. The technique is illustrated in Fig. 8.

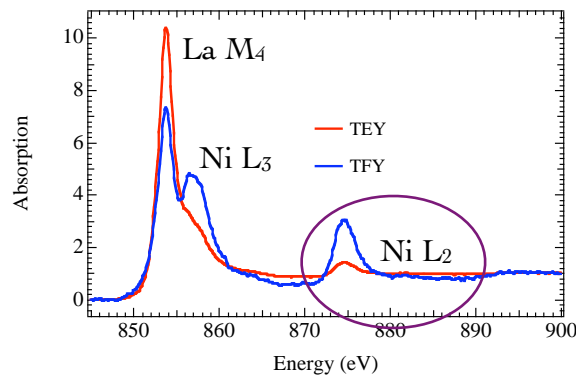


Figure 7. XAS spectrum showing Ni valency in the superlattice consistent with perfect bulk like Ni^{3+} valency.

In complete expectation with the theoretical prediction we clearly observed the orbital re-occupation of the initially degenerate eg electron due to the strong changes in the crystal field

Resonant XLD at Ni L2-edge

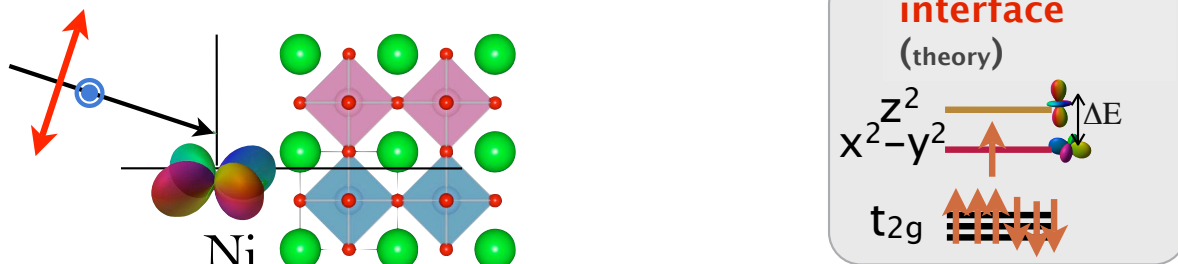


Figure 8. Schematic of the XLD technique, which uses the polarization vector, aligned along and across the atomic orbital in question to probe its symmetry.

caused by the epitaxial growth on SrTiO₃ (001) substrate with much larger lattice parameter (about 3.2% lattice mismatch). As clearly seen for the case of the superlattice grown on STO the initially degenerate orbitals split by about 20%, at the same time as a control measurement the films grown on LAO where the expected lattice mismatch is small -0.8% we observe a very small orbital reconstruction (see Fig. 11). At the same time there is a clear shift in the energy position of the L2 absorption edge thus signalling about the d-band splitting for the sample grown on LAO!

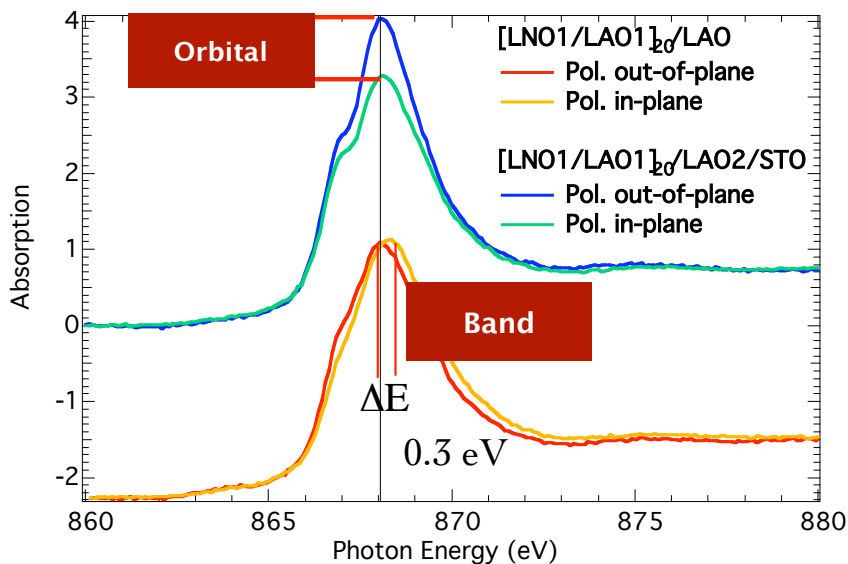


Figure 9. Linearly polarized XAS spectra taken at the L2 edge show the effect of strain.

This observation is rather unexpected, since naively one would expect that there would be no such a large difference in the behaviour between the compressive and tensile strain. A possible key to the puzzle why the compressive LAO strain induces the d-band splitting is in the profoundly different arrangement of atoms at the interface. Recap that LAO possesses a rhombohedral crystal structure R3-c whereas STO is cubic of Pm-3m. It is interesting to assume

that since LNO is of R3-c symmetry which perfectly matches the symmetry of LAO the arrangement of bridging oxygen atoms at the interface would be close to that of the bulk, whereas this is clearly not the case when having a cubic atom arrangement placed against the rhombohedral lattice of LNO. The position of oxygen atoms would be dramatically different in this case and structurally the interface will result in multiple domains to keep the atoms in registry.

Summary. This issue of the symmetry accommodation is completely unaddressed and will naturally have dramatic consequences for the electronic properties (e.g. transport, heat capacitance etc.). The work in this direction is now in progress in close collaboration with Dr. Phil Ryan from APS, ANL.